

Particle coalescing with angular momentum conservation in SPH simulations

Balázs Tóth

Department of Hydraulic and Water Resources Engineering, Budapest University of Technology and Economics

Abstract

The present work introduces a simple, yet effective particle coalescing procedure for two-dimensional SPH simulations with adaptive spatial resolution. In addition to the regular conservation properties of former algorithms concerning the mass and linear momentum, the current model provides the exact conservation of the angular momentum as well. The detailed discussion of the coalescing method is followed by its verification through a frozen Taylor-Green vortex example with gradually derefined particle configuration. As a demonstration of the applicability of the proposed technique, a typical weakly compressible dam-break simulation with adaptive resolution is presented and comparisons are made for uniformly coarse and refined resolutions.

Keywords: smoothed particle hydrodynamics, adaptive resolution, particle coalescing, momentum conservation

1. Introduction

In computational science, it is highly common during the approximate solution of partial differential equations, that some requirements significantly vary in the computational domain, such as the accuracy or the level of detail of the numerical simulation results. Thus, the application of spatially varying numerical resolution plays crucial role in cost reduction of simulations, especially in computational fluid dynamics (CFD). Mesh-based finite volume (FVM) and even finite element methods (FEM) provide robust spatial adaptivity remarkably reducing the computational costs for simulations of several applications [1]. Similarly, in case of particle-based Lagrangian

methods adaptive resolution is also desirable, though the implementation of those models lies on slightly different assumptions.

One of the most fundamental and frequently referred meshless numerical technique is the Smoothed Particle Hydrodynamics (SPH) scheme. The first model using SPH has been constructed by Gingold and Monaghan in 1977 [2] and independently in the same year by Lucy [3]. Initially, the method was developed for simulating astrophysical phenomena, implying large-scale self-gravitating gaseous systems in absence of boundary conditions. Later, exploiting the special properties of SPH, the method has been successfully applied for the simulation of both solid and fluid phases [4, 5], making SPH recently an increasingly applied theory in ocean engineering and several other fields [6–8]. Although the theory behind the variable smoothing lengths of the particles in SPH had been long since formulated [9, 10], in order for the resolution in a specific region to be increased, particles need to be properly inserted and removed from the computational domain.

Based on different approaches, several techniques for adaptive resolution have been introduced during the past two decades. Firstly, [11] presented a particle splitting method for astrophysical simulations while [12] achieved locally increased resolution using a Delaunay triangulation. Later, [13] constructed criteria for local particle addition and removal with the interpolation of flow conditions and the distribution of particle mass. The precise splitting technique presented in [14] became one of the most widely used methods developed further in [15–19] and extended for shallow water formulations in [20, 21]. As a noteworthy idea, [22] applied the same splitting scheme but without the deletion of the mother particles. Instead by turning them into passive tracers, they can be implied in the flow again later, and the daughter particles can be simply deleted when leaving the high-resolution zone.

Most recently, another approach in adaptive resolution is based on the coupling of different fluid simulations [23, 24] as a realization of a coupling of SPH fluid flows of different particle sizes. Such implementations are presented in [25–27], SPH domains are overlapped through a buffer zone, in which fluid conditions are being interpolated between the zones using a set of spatially fixed interfacial particles.

According to the knowledge of the author, none of the existing particle coalescing techniques within the SPH framework offer the conservation of angular momentum. Regardless of the coarsening procedure, the aforementioned techniques reduce the degrees of freedom of the original configuration so that the angular momentum inevitably vanishes in the merged or dere-

finer configuration. In the present work, a particle coalescing technique is introduced, which exactly preserves not only the mass and the linear momentum, but the angular momentum as well without significant additional computational cost compared to the existing methods.

2. Motivation

The particle merging process introduced in [28] performs coalescing of particle pairs in such a way that a candidate particle a and its closest neighbor b are replaced with a new particle m in the common center of mass of particles a and b . As it has been shown in [28], pairwise coalescing process can be formulated so that mass and linear momentum are exactly preserved. However, during the merge, the degrees of freedom of the local particle set $\{a, b\}$ and $\{m\}$ is reduced from 4 to 2 in two dimensions. As a result, in case of the velocity vectors of the original pair of particles are not equal ($\mathbf{v}_a \neq \mathbf{v}_b$), the merge leads to a complete loss of angular momentum. The basic idea

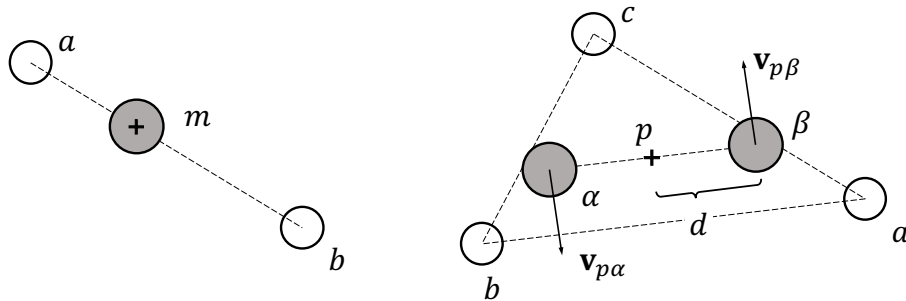


Figure 1: Coalescing of a particle pair (left) and a triplet (right). The original and the new particle layout are shown by the empty and shaded circles respectively.

behind the proposed resolution reduction technique is that in two dimensions the angular momentum can be preserved only if the remaining degrees of freedom after merging is at least 4. Thus, in the present work we introduce a modified particle coalescing technique in which the particle merging is performed over particle triplets instead of pairs. The difference between the two methods is shown in Figure 1. After merging, a triplet $\{a, b, c\}$ is replaced with a pair of identical particles $\{\alpha, \beta\}$, reducing the initial degrees of freedom from 6 to 4, which is still sufficient to preserve both the local linear and angular momenta of the original layout.

3. The merging procedure

3.1. Conservation of mass and linear momentum

Before placing the new particles, the position and velocity of the center of mass of the particles to be merged need to be computed. Furthermore, by keeping these quantities the same before and after the merge, the linear momentum is also preserved. As a result, we require, that:

$$\begin{aligned}\mathbf{r}_p &= \frac{\mathbf{r}_a m_a + \mathbf{r}_b m_b + \mathbf{r}_c m_c}{m_a + m_b + m_c} = \frac{\mathbf{r}_\alpha m_\alpha + \mathbf{r}_\beta m_\beta}{m_\alpha + m_\beta}, \\ \mathbf{v}_p &= \frac{\mathbf{v}_a m_a + \mathbf{v}_b m_b + \mathbf{v}_c m_c}{m_a + m_b + m_c} = \frac{\mathbf{v}_\alpha m_\alpha + \mathbf{v}_\beta m_\beta}{m_\alpha + m_\beta}.\end{aligned}\tag{1}$$

The exact conservation of mass is also enforced by choosing the new masses as

$$m_\alpha = m_\beta = m_m = \frac{m_a + m_b + m_c}{2}.\tag{2}$$

3.1.1. Computing the smoothing length and the new positions

To minimize the influence of the change in the particle layout on the solution, the minimization of the density variation during particle splitting and coalescing is of crucial importance [14]. In attempt to minimize the change in the density field, we compute the density at \mathbf{r}_p for both the original and coalesced layout, which therefore should be equal:

$$\rho_p = \sum_{i=a,b,c} m_i W(|\mathbf{r}_p - \mathbf{r}_i|, h_i) = (m_\alpha + m_\beta)(W(|\mathbf{r}_p - \mathbf{r}_\alpha|, h_\alpha)) = (m_\alpha + m_\beta)W_{\alpha p},\tag{3}$$

where for the sake of simplicity of the subsequent assumptions, we consider the two-dimensional Gaussian smoothing kernel function

$$W(r, h) = \frac{1}{\pi h^2} \exp\left(-\frac{r^2}{h^2}\right).\tag{4}$$

In contrast with [28], the smoothing radius cannot be computed directly due to $r \neq 0$ takes place in (4). Furthermore, as it is visualized in Figure 2, normalized kernels cannot produce arbitrary high values at a given place by varying the smoothing radius, therefore the distance $d = |\mathbf{r}_\alpha - \mathbf{r}_\beta|/2$ should be chosen carefully to avoid infeasible solutions of (3). To compute the maximum distance $r_{max} = |\mathbf{r}_\alpha - \mathbf{r}_p|$, at which (3) can be satisfied, (4) has

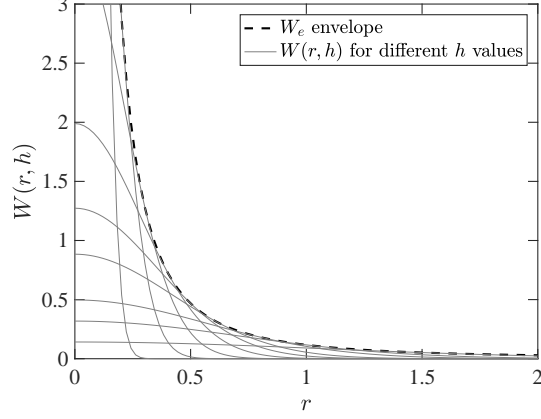


Figure 2: Gaussian kernel functions with different smoothing radii (gray solid curves) and the envelope (black dashed curve) marking the maxima of x for the corresponding values of $W(x, h)$.

been analytically analysed. Firstly, using the known value of $W_{\alpha p}$ from (3), consider the inverse of the Gaussian kernel function:

$$r = \sqrt{h^2 \ln(W_{\alpha p} \pi h^2)}. \quad (5)$$

To find its maxima, the derivative with respect to the smoothing length is computed and constrained to zero as follows

$$\frac{\partial r}{\partial h} = -\frac{\ln(W_{\alpha p} \pi h^2) + 1}{\sqrt{\ln(W_{\alpha p} \pi h^2)}} = 0. \quad (6)$$

This equation has finite roots only if the numerator is zero, thus the solution of

$$\ln(W_{\alpha p} \pi h^2) = -1 \quad (7)$$

gives

$$h_{max} = \sqrt{\frac{1}{e\pi W_{\alpha p}}}, \quad (8)$$

which is then the smoothing length corresponding to the maximum value of the distance r_{max} for a given value of W . Finally, substituting h_{max} to (5) gives

$$r_{max} = \sqrt{-\frac{1}{e\pi W_{\alpha p}} \ln\left(\frac{W_{\alpha p} \pi}{e\pi W_{\alpha p}}\right)} = \sqrt{\frac{1}{e\pi W_{\alpha p}}} = h_{max}, \quad (9)$$

which yields that $x = h$ is a nullcline of (6) for arbitrary W , shown in Figure 3. From (9), the envelope Figure 2 of the Gaussian kernel can be expressed as

$$W_e = \frac{1}{e\pi x^2}. \quad (10)$$

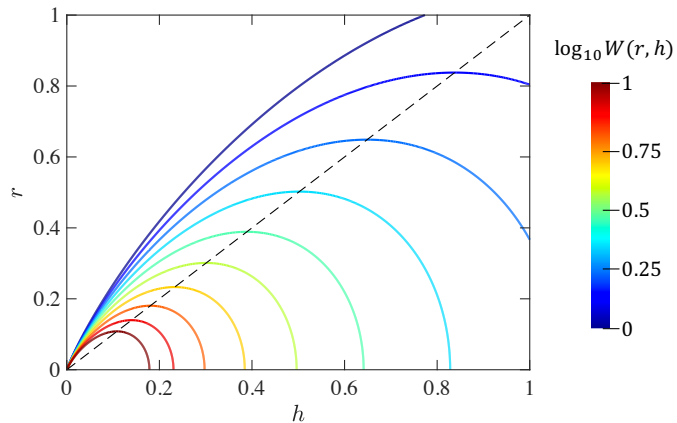


Figure 3: Isocurves of the Gaussian kernel on the $r - h$ plane (solid lines), and the $r = h$ nullcline (dashed line).

Although the maximum distance $r_{max} = |\mathbf{r}_\alpha - \mathbf{r}_p|$ can be computed from the simple expression (9), the optimal distance is usually smaller. In the present work, the new spacing was chosen to be equal to the average distance of the original particles from \mathbf{r}_p :

$$d = \eta \frac{1}{3} \sum_{i=a,b,c} |\mathbf{r}_i - \mathbf{r}_p|, \quad (11)$$

where η is a scaling constant, which results a uniform particle distribution when set between 0.9 and 1, and d limited to r_{max} only if $d \geq r_{max}$. Otherwise the smoothing radius $h_\alpha = h_\beta$ needs to be computed. Since (4) cannot be solved directly for h , the iterative solution

$$h^{n+1} = \sqrt{\frac{1}{\pi W_{\alpha p}} \exp\left(-\frac{r^2}{(h^n)^2}\right)} \quad (12)$$

is used, where the superscript denotes the iteration level and $h^0 = h_{max}$. The iteration is terminated if the

$$10^{-6} > \frac{h^n - h^{n+1}}{h^n} \quad (13)$$

exiting criterion is satisfied.

After computing the distance d and smoothing radius h , the positions \mathbf{r}_α and \mathbf{r}_β are obtained using the simple constraint

$$\mathbf{r}_\alpha - \mathbf{r}_\beta \parallel \max(\mathbf{r}_{ab}, \mathbf{r}_{ac}, \mathbf{r}_{bc}). \quad (14)$$

3.2. Conservation of angular momentum

The linear momentum is exactly preserved if the

$$\sum_{i=a,b,c} m_i \mathbf{v}_i = m_\alpha \mathbf{v}_\alpha + m_\beta \mathbf{v}_\beta = m_m (\mathbf{v}_\alpha + \mathbf{v}_\beta) = (m_\alpha + m_\beta) \mathbf{v}_p \quad (15)$$

condition is satisfied. Considering the center of mass instead of the origin, (15) can be written in relative coordinates, implying that the linear momentum vanishes in the co-moving frame:

$$\sum_{i=a,b,c} m_i \mathbf{v}_{pi} = m_\alpha \mathbf{v}_{p\alpha} + m_\beta \mathbf{v}_{p\beta} = m_m (\mathbf{v}_{p\alpha} + \mathbf{v}_{p\beta}) = 0, \quad (16)$$

which in turn yields to

$$\mathbf{v}_{p\alpha} = -\mathbf{v}_{p\beta}. \quad (17)$$

Thus, compared to [28], the degrees of freedom additionally implied in our model can be exploited to carry non-zero velocities without violating the linear momentum conservation.

Similarly to (16), the angular momentum conservation can be expressed in the co-moving frame. Considering that the particle layout and merging process is being performed in two dimensions, the angular momentum becomes a scalar quantity. Using (17), the angular momentum in terms of the center of mass reads as

$$\sum_{i=a,b,c} m_i (\mathbf{r}_{ip} \times \mathbf{v}_{ip}) \mathbf{e}_k = (m_\alpha \mathbf{r}_{\alpha p} \times \mathbf{v}_{\alpha p} + m_\beta \mathbf{r}_{\beta p} \times \mathbf{v}_{\beta p}) \mathbf{e}_k = (m_\alpha + m_\beta) (\mathbf{r}_{\alpha p} \times \mathbf{v}_{\alpha p}) \mathbf{e}_k, \quad (18)$$

which can be directly applied to compute the velocities $\mathbf{v}_{\alpha p}$ and $\mathbf{v}_{\beta p}$, hence the velocities in the global frame read as

$$\mathbf{v}_\alpha = \mathbf{v}_{\alpha p} + \mathbf{v}_p = -\mathbf{v}_\beta. \quad (19)$$

4. Fluid flow modeling with SPH

This section briefly presents the most fundamental and conventional fluid flow model of the Lagrangian particle-based SPH method applied in the present work.

4.1. Governing equations

Considering the substantial or material time-derivative of any quantity A as the sum of the local and convective terms

$$\frac{dA}{dt} = \frac{\partial A}{\partial t} + \mathbf{v} \cdot \nabla A, \quad (20)$$

the governing equations of an arbitrary, compressible inviscid fluid can be written in the Lagrangian frame:

$$\begin{aligned} \frac{d\rho}{dt} &= -\rho \nabla \cdot \mathbf{v}, \\ \frac{d\mathbf{v}}{dt} &= -\frac{1}{\rho} \nabla p + \mathbf{g} + \frac{\mathbf{f}}{\rho_i}, \end{aligned} \quad (21)$$

where ρ , p , \mathbf{v} and \mathbf{f} are the density, pressure, velocity and the sum of the specific external forces respectively and \mathbf{g} is the gravitational acceleration vector. In the present work the weakly compressible variant of SPH is used to control compressibility with the equation of state

$$p = c^2(\rho - \rho_0), \quad (22)$$

where c is the artificially reduced speed of sound and ρ_0 is the reference density of the fluid. The speed of sound is usually tuned to keep the maximum density variations around 1% using the following condition:

$$c = 10v_{max}, \quad (23)$$

where v_{max} is the expected maximum of the velocity magnitude in the specific flow problem.

4.2. The SPH discretization

SPH is a pure Lagrangian meshless collocation method for the solution of time-dependent partial differential equations (PDEs) such as (21). The

fundamental idea is that any function A can be reconstructed in the domain Ω using the generalized interpolation also known as convolution

$$A(\mathbf{r}) = \int_{\Omega} A(\mathbf{r} - \mathbf{r}') \delta(\mathbf{r} - \mathbf{r}') d\mathbf{r}, \quad (24)$$

which, after changing the Dirac-function $\delta(\mathbf{r} - \mathbf{r}')$ to an appropriate mollifier $W_{ij} = W(|\mathbf{r}_i - \mathbf{r}_j|)$, can be written for finite-size nodes (particles) in discrete form as

$$\langle A(\mathbf{r}_i) \rangle = \langle A_i \rangle = \sum_j A_j W_{ij} \frac{m_j}{\rho_j}, \quad (25)$$

where m_j and ρ_j are the mass and density assigned to particle j .

The expression (25) can be used for the construction of the algebraic approximation of local spatial derivatives such as gradient and divergence of any function. Thus, according to [29], the pressure gradient and the divergence of the velocity field can be written as

$$\begin{aligned} \langle \nabla p_i \rangle &= \rho_i \sum_j \left(\frac{p_i}{\rho_i^2} + \frac{p_j}{\rho_j^2} \right) \nabla W_{ij} \frac{m_j}{\rho_j}, \\ \langle \nabla \cdot \mathbf{v}_i \rangle &= \sum_j (\mathbf{v}_j - \mathbf{v}_i) \nabla W_{ij} \frac{m_j}{\rho_j}. \end{aligned} \quad (26)$$

Through the conventional SPH discretization process, the PDE system (21) is converted into a set of ordinary differential equations (ODE's) by substituting the spatial derivatives with the SPH algebraic representations. Thus, the conventional SPH fluid-equations read as

$$\begin{aligned} \frac{d\rho_i}{dt} &= -\rho_i \sum_j (\mathbf{v}_j - \mathbf{v}_i) \frac{m_j}{\rho_j} \nabla W_{ij}, \\ \frac{d\mathbf{v}_i}{dt} &= -\sum_j \left(\frac{p_i}{\rho_i^2} + \frac{p_j}{\rho_j^2} \right) m_j \nabla W_{ij} + \mathbf{g} + \frac{\mathbf{f}_i}{\rho_i}, \end{aligned} \quad (27)$$

where the subscripts denote particle i and its neighbouring particles j and $W_{ij} = W(\mathbf{r}_i - \mathbf{r}_j, h)$ is chosen to be the fifth order polynomial Wendland smoothing kernel function:

$$W(q) = \begin{cases} C_d (1 - \frac{q}{2})^4 (2q + 1) & \text{if } q \leq 2 \\ 0 & \text{if } q > 2 \end{cases}, \quad (28)$$

where $q = |\mathbf{r}_{ij}|/h$, $C_d = 7/(4\pi h^2)$ is the normalization constant in two dimensions and h is the smoothing radius. In the present work, the interparticle distance is chosen to be $dx = 2.1h$.

To facilitate numerical stability and reduce spurious oscillations in the solution, the equations (27) are usually extended by artificial diffusive terms. Here, the stabilization terms presented in [30] are applied for both the continuity and momentum equations, hence the whole system reads as:

$$\begin{aligned} \frac{d\rho_i}{dt} &= -\rho_i \sum_j (\mathbf{v}_j - \mathbf{v}_i) \frac{m_j}{\rho_j} \nabla W_{ij} + \xi hc \sum_j \Psi_{ij} \nabla W_{ij} \frac{m_j}{\rho_j}, \\ \frac{d\mathbf{v}_i}{dt} &= -\sum_j \left(\frac{p_i}{\rho_i^2} + \frac{p_j}{\rho_j^2} \right) m_j \nabla W_{ij} + \mathbf{g} + \frac{\mathbf{f}_i}{\rho_i} + \alpha hc \rho_0 \sum_j \pi_{ij} \nabla W_{ij} \frac{m_j}{\rho_j}, \\ p_i &= c^2(\rho_i - \rho_0), \end{aligned} \quad (29)$$

where $\xi = 0.1$ and $\alpha = 0.01$ are diffusion constants and

$$\begin{aligned} \Psi_{ij} &= 2(\rho_j - \rho_i) \frac{\mathbf{r}_{ji}}{|\mathbf{r}_{ji}|^2}, \\ \pi_{ij} &= (u_j - u_i) \frac{\mathbf{r}_{ji}}{|\mathbf{r}_{ji}|^2}. \end{aligned} \quad (30)$$

5. Results and discussion

5.1. Frozen Taylor-Green vortex

A simple case for verification of the angular momentum conservation is the investigation of a single, high resolution vortex under gradual derefinement without the presence of physical or artificial dissipation. For the initial layout, we constructed a 209×209 grid of particles in an axis-aligned origin-centered unit square with the velocity field given by the velocity field of the Taylor-Green vortex sheet

$$\mathbf{v} = \begin{bmatrix} \sin(\pi(x - 0.5))\cos(\pi(y - 0.5)) \\ -\cos(\pi(x - 0.5))\sin(\pi(y - 0.5)) \end{bmatrix}. \quad (31)$$

Without moving the Lagrangian particles in space due to their velocities, the initial layout has been gradually derefined until the number of particles reached the order of magnitude of 10, which is considered to be a coarse representation of a vortex. As Figure 4 shows, similarly to the conventional

particle coalescing techniques, the uniformity of the particle layout is preserved during the derefinement process. In turn, presented in Figure 5, the merging process based on the particle triplets preserves the angular momentum exactly. In comparison with pairwise coalescing techniques, our method reduces the particle number in every derefinement step with the theoretical maximum rate of 33.3% instead of 50%. As it is visible in Figure 5, this moderate reduction rate causes the increment of the required steps (from 20 to 30 in this specific case) until reaching the desired coarse resolution.

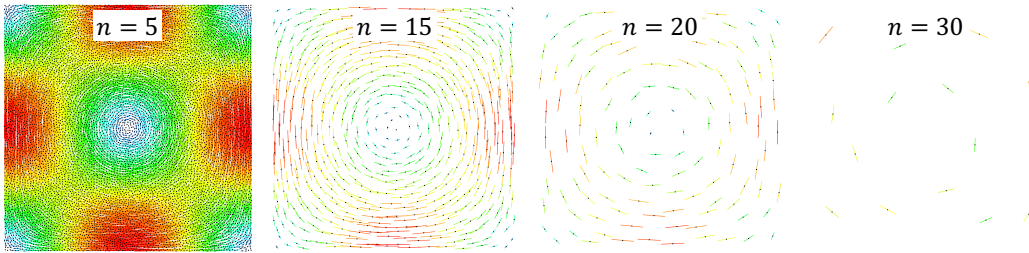


Figure 4: Particle layout during the resolution coarsening with our derefinement technique. n shows the number of derefinement steps performed from the initial grid.

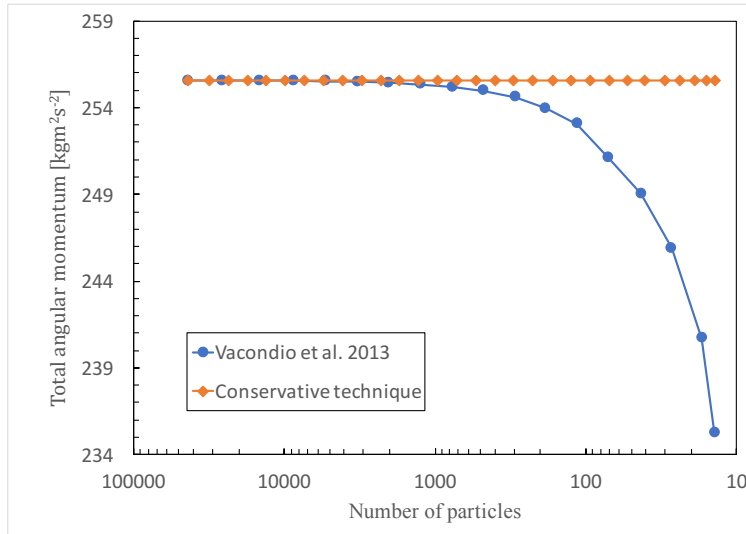


Figure 5: Total angular momentum of the vortex as a function of the number of particles while sequentially merging pairs (blue line with circles) and triplets (orange line with diamonds).

5.2. Two-dimensional dam-break

In the second test case, the applicability of the proposed method is demonstrated by a two-dimensional dam-break simulation. The initial geometrical layout is shown in Figure 6. Using spatially fixed fluid particles, the walls of the tank were built up as a uniform grid. For the adaptive spatial resolution, a rectangular region with higher desired resolution was considered in the bottom right corner. Particles entering this region had been split up to 7 refined or daughter particles following the pattern presented in [14]. During the splitting, the number of daughter particles were $n_d = 7$, the separation parameter and smoothing ratio were set to $\epsilon = 0.4$ and $\alpha = 1/\sqrt{n_d}$ respectively. According to the merging algorithm, once a refined particle leaves and moves apart from the region farther than the initial coarse interparticle distance dx , it is marked as a candidate for coalescing and potentially merged with two of the closest particles in the neighborhood. It is important to note that new particles do not participate in further coalescing in the same time step. During the sequence of the derefinement steps, small particles gradually restore the original coarse spatial resolution. Coloring the particles according to their pressure values, four different time instants of the simulation results with the locally increased resolution are visible in Figure 7.

Besides the computation with the dynamic resolution, two further simulations were performed using uniformly coarse ($H = 42dx$) and fine resolutions ($H = 111dx$) as well. For comparison, the time series of the pressure had been evaluated at the probe on the right side of the tank marked with a red dot in Figure 6. To eliminate non-physical numerical oscillations, a fixed size ($\Delta = 0.04$ s) moving average filter was applied on the pressure time series for each simulation result. Considering the high-resolution case to be accurate, the quadratic difference for the coarse and adaptive resolutions are shown in Figure 8. The root mean square errors (RMSE)

$$\sigma = \sqrt{\frac{(P - p_i)}{N_t}}, \quad (32)$$

were also computed, where, P is the pressure series evaluated at the wall in the high resolution case and $N_t = 200$ is the length of the time series. The RMSE results of the coarse and adaptive resolutions $\sigma_c = 441.32$ Pa and $\sigma_a = 256.96$ respectively yield the considerable improvement in the accuracy with moderate additional computational requirement.

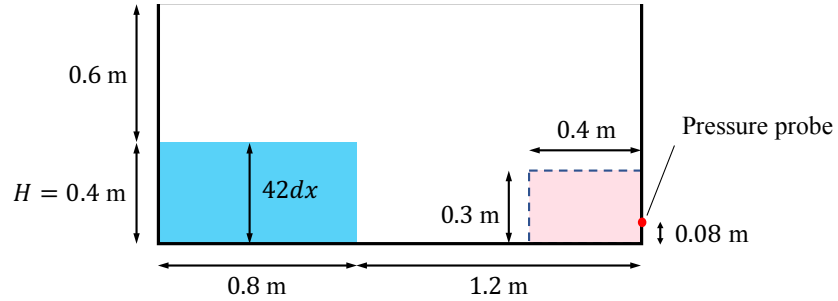


Figure 6: Initial condition of the two-dimensional dam-break problem. High-resolution region is visualized with the light red rectangle in the right corner, while the red dot marks a pressure probe. The initial interparticle distance is denoted by dx .

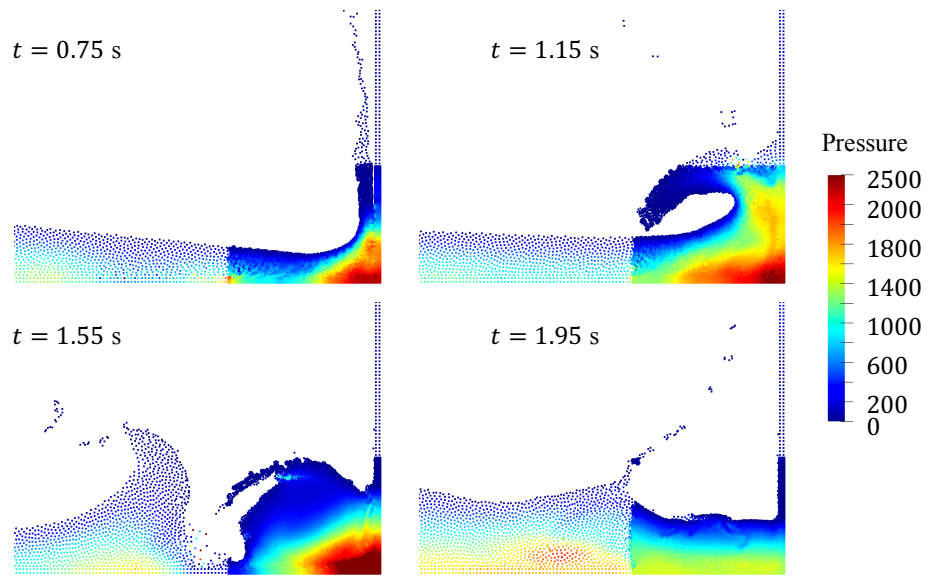


Figure 7: Dam-break with dynamic splitting and conservative merging in the bottom right corner.

6. Implementation

The proposed conservative model and the simulation cases in the present work have been implemented and run in Nauticle [31], the general purpose particle-based parallel simulation tool facilitating the application and development of meshless numerical methods.

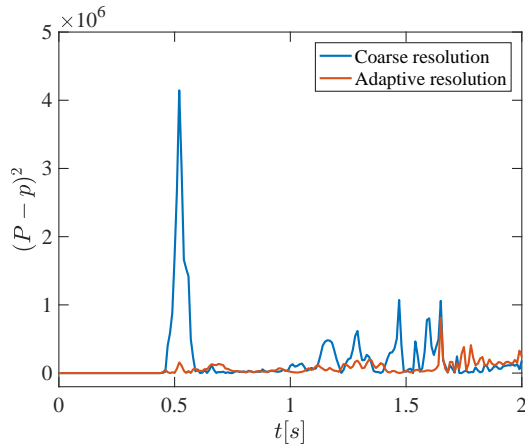


Figure 8: Quadratic pressure deviation of the coarse (blue and dashed line) and adaptive (orange solid line) simulations from the fine resolution.

7. Conclusion

A novel coalescing technique with exact angular momentum conservation is introduced. The method can be considered as an extension of the former pairwise merging techniques, however, some nontrivial steps are required. During the derefinement of high resolution particles, former merging techniques replace a pair of particles with a single one inevitably canceling out local rotational motion and consequently the angular momentum. In this work, to preserve angular momentum, additional degrees of freedom for the coalesced layout are achieved by replacing three particles instead of two with a pair of identical co-rotating particles. The smoothing radius of the coalesced particles is obtained with the inverse of the Gaussian kernel so that the density error is eliminated in the local center of mass of the particles.

The proposed method has been verified through a frozen Taylor-Green vortex example with several consecutive derefinement steps from high to low resolutions. It has been shown, that pairwise techniques suffer from significant loss of angular momentum when the resolution of the vortex becomes low. Moreover, to demonstrate the efficiency of the new particle replacement scheme a two-dimensional adaptive dam-break simulation has been compared to simulations with uniformly coarse and fine resolutions.

Since the proposed enhancement requires only a few additional computationally cheap steps compared to pairwise methods, its application is feasible in most circumstances, and even extendable to three dimensions.

References

- [1] M. J. Berger, P. Colella, Local adaptive mesh refinement for shock hydrodynamics, *Journal of computational Physics* 82 (1) (1989) 64–84.
- [2] R. Gingold, J. Monaghan, Smoothed particle hydrodynamics theory and application to non-spherical stars, *Mon. Not. R. Astron. Soc.* vol. 181 (1977) 375–389.
- [3] L. Lucy, A numerical approach to the testing of the fission hypothesis, *Astron. J.* vol. 82 (1977) 1013–1024.
- [4] J. Monaghan, Simulating free surface flows with sph, *J. Comput. Phys.* 110 (1994) 399–406.
- [5] J. Gray, J. Monaghan, R. Swift, Sph elastic dynamics, *Comput. Methods Appl. Mech. Eng.* 190 (2001) 6641 – 6662.
- [6] S. Chowdhury, S. Sannasiraj, SPH Simulation of shallow water wave propagation, *Ocean Engineering* 60 (2013) 41–52. doi:10.1016/j.oceaneng.2012.12.036.
- [7] R. Dalrymple, B. Rogers, Numerical modeling of water waves with the SPH method, *Coastal Engineering* 53 (2006) 141–147. doi:10.1016/j.coastaleng.2005.10.004.
- [8] X. Sun, M. Sakai, Y. Yamada, Three-dimensional simulation of a solid-liquid flow by the DEM-SPH method, *Journal of Computational Physics* 248 (2013) 147–176. doi:10.1016/j.jcp.2013.04.019.
- [9] R. Gingold, J. Monaghan, Kernel estimates as a basis for general particle methods in hydrodynamics, *Journal of Computational Physics* 46 (3) (1982) 429–453.
- [10] J. Monaghan, Sph compressible turbulence, *Monthly Notices of the Royal Astronomical Society* 335 (3) (2002) 843–852.
- [11] S. Kitsionas, A. Whitworth, Smoothed particle hydrodynamics with particle splitting, applied to self-gravitating collapse, *Monthly Notices of the Royal Astronomical Society* 330 (1) (2002) 129–136.

- [12] G.-R. Liu, Mesh free methods: moving beyond the finite element method, CRC press, 2002.
- [13] M. Lastiwka, N. Quinlan, M. Basa, Adaptive particle distribution for smoothed particle hydrodynamics, *International Journal for Numerical Methods in Fluids* 47 (10-11) (2005) 1403–1409.
- [14] J. Feldman, J. Bonet, Dynamic refinement and boundary contact forces in sph with applications in fluid flow problems, *International Journal for Numerical Methods in Engineering* 72 (3) (2007) 295–324.
- [15] Y. R. López, D. Roose, Particle refinement for fluid flow simulations with sph, *Computer Methods in Mechanics*, CMM-2011, Warsaw, Poland.
- [16] R. Vacondio, B. Rogers, P. Stansby, P. Mignosa, Variable resolution for sph in three dimensions: Towards optimal splitting and coalescing for dynamic adaptivity, *Computer Methods in Applied Mechanics and Engineering* 300 (2016) 442–460.
- [17] W. Liu, P. Sun, F. Ming, A. Zhang, Application of particle splitting method for both hydrostatic and hydrodynamic cases in sph, *Acta Mechanica Sinica* (2017) 1–13.
- [18] L. Wang, F. Xu, Y. Yang, J. Wang, A dynamic particle refinement strategy in smoothed particle hydrodynamics for fluid–structure interaction problems, *Engineering Analysis with Boundary Elements*.
- [19] Q. Xiong, B. Li, J. Xu, Gpu-accelerated adaptive particle splitting and merging in sph, *Computer Physics Communications* 184 (7) (2013) 1701–1707.
- [20] R. Vacondio, B. Rogers, P. Stansby, Accurate particle splitting for smoothed particle hydrodynamics in shallow water with shock capturing, *International Journal for Numerical Methods in Fluids* 69 (8) (2012) 1377–1410.
- [21] R. Vacondio, B. Rogers, P. Stansby, P. Mignosa, Shallow water sph for flooding with dynamic particle coalescing and splitting, *Advances in Water Resources* 58 (2013) 10–23.

- [22] D. A. Barcarolo, D. Le Touzé, G. Oger, F. De Vuyst, Adaptive particle refinement and derefinement applied to the smoothed particle hydrodynamics method, *Journal of Computational Physics* 273 (2014) 640–657.
- [23] B. Bouscasse, S. Marrone, A. Colagrossi, A. D. Mascio, Multi-purpose interfaces for coupling sph with other solvers, in: *Proceedings of the 8th International SPHERIC Workshop*, 2013.
- [24] S. Marrone, A. Di Mascio, D. Le Touzé, Coupling of smoothed particle hydrodynamics with finite volume method for free-surface flows, *Journal of Computational Physics* 310 (2016) 161–180.
- [25] X. Bian, Z. Li, G. E. Karniadakis, Multi-resolution flow simulations by smoothed particle hydrodynamics via domain decomposition, *Journal of Computational Physics* 297 (2015) 132–155.
- [26] W. Hu, W. Pan, M. Rakhsha, Q. Tian, H. Hu, D. Negrut, A consistent multi-resolution smoothed particle hydrodynamics method, *Computer Methods in Applied Mechanics and Engineering* 324 (2017) 278–299.
- [27] L. Chiron, G. Oger, M. De Leffe, D. Le Touzé, Analysis and improvements of adaptive particle refinement (apr) through cpu time, accuracy and robustness considerations, *Journal of Computational Physics* 354 (2018) 552–575.
- [28] R. Vacondio, B. Rogers, P. Stansby, P. Mignosa, J. Feldman, Variable resolution for sph: a dynamic particle coalescing and splitting scheme, *Computer Methods in Applied Mechanics and Engineering* 256 (2013) 132–148.
- [29] J. Monaghan, Smoothed particle hydrodynamics, *Rep. Prog. Phys.* vol. 68 (2005) 1–34.
- [30] Free-surface flows solved by means of sph schemes with numerical diffusive terms, *Computer Physics Communications* 181 (3) (2010) 532 – 549.
- [31] B. Tóth, Nauticle: a general-purpose particle-based simulation tool, CoRR abs/1710.08259. [arXiv:1710.08259](https://arxiv.org/abs/1710.08259).
URL <http://arxiv.org/abs/1710.08259>